Wake measurement metrics and the dependence of tidal turbine wakes on turbine operating condition

T. Ebdon*‡, D.M. O'Doherty †, T. O'Doherty *§, A. Mason-Jones *¶
*School of Engineering, Cardiff University, Cardiff, United Kingdom
‡EbdonT@cardiff.ac.uk
§odoherty@cardiff.ac.uk
¶Mason-JonesA@cardiff.ac.uk
†odoherty394@gmail.com

***Abstract*—Metrics are introduced for measuring the length and width of a turbine wake. These metrics are closely examined, and their relative advantages and disadvantages are discussed. Following this, a CFD study is carried out for a model-scale tidal turbine over a wide range of tip-speed ratios, and the performance and wake of the turbine is analysed. The study indicates that wake length is relatively unaffected by the turbine operating condition beyond the near wake, but that wake widths appear to be closely related to the turbine operating condition.**

NOMENCLATURE

A	=	rotor swept area, m^2
C_P	=	power coefficient
C_T	=	thrust coefficient
C_θ	=	torque coefficient
D	=	rotor diameter, m
F_t	=	thrust force on turbine, N
G_ϕ	=	axial flux of angular momentum
G_x	=	axial flux of linear momentum, m^{-1}
r	=	turbine radius, m
S	=	swirl number
u	=	instantaneous velocity, m/s
u_i'	=	fluctuating velocity i direction, m/s
U	=	average velocity, m/s
v	=	free-stream velocity, m/s
λ	=	tip-speed ratio
ρ	=	fluid density, kg/m^3
τ	=	turbine torque, Nm
τ_{ij}	=	stress component acting in j direction on surface normal to i direction, N/m^2
ω	=	turbine angular velocity, rad^{-1}

I. INTRODUCTION

Calculations have shown the potential for tidal stream turbines to provide a reliable, constant base-load for the UK energy supply. This could be achieved by siting arrays of tidal turbines at strategic points around the British Isles, in order to utilise the time-difference of the tidal phase[1]. The nature of the tidal flow around the British Isles means that one or more sites would always be at near peak flow, thus providing a reliable source of low-carbon energy. However, the regions of the sea bed which lend themselves to the installation and operation of tidal turbines are limited in geographical extent due to both hydrodynamic considerations (flow velocity, local turbulence), as well as practical considerations (depth of water, suitability of sea bed, proximity to coast, shipping lanes etc). Given the need to extract as much energy as possible from these limited geographical regions, it is probable that tidal turbines will be deployed in arrays; groups of turbines in close proximity to one another. With turbines being grouped in this way, it is to be expected that their close proximity will lead to hydrodynamic inter-turbine interactions. These may have a positive effect on energy extraction due to blockage effects and flow acceleration[2], but could also have a negative effect on each other, due to less energy being available for the downstream turbines, or increased turbulence in the flow leading to unacceptable structural demands being placed on downstream turbines[3]. Whilst work has been done in the field of wind farm layout optimisation, there is greater potential for optimisation benefits in the tidal industry, due to the highly predictable and periodic nature of the flow.

Crucial to obtaining a necessary understanding of inter-turbine interactions is the ability to accurately model tidal turbine wakes under a variety of flow and operating conditions. To date, the majority of numerical studies of both tidal and wind turbines have used Reynolds-Averaged Navier-Stokes (RANS) models, with some using Blade Element Momentum Theory (BEMT). These models have been shown to be able to accurately predict turbine performance characteristics (power output, torque output, thrust), when compared to measurements obtained in low-turbulence flume measurements, and zero-turbulence tow tank experiments. However, these models struggle to predict the length of the turbine wakes. Some studies have attempted to overcome the limitations of RANS turbulence modelling by directly resolving the large scale turbulence using Large Eddy Simulation (LES). However, due to the high computational requirements associated with LES modelling, these studies have either used a limited spatial domain[4], or have simplified the turbine geometry by using actuator lines[5] or discs[6] to reduce computational requirements. These simplifications allow the effects of large-scale turbulence to be accounted for, but at the cost of either not providing a solution for the entire wake region of interest, or by simplifying the turbine geometry which means that effects of the flow on the turbine itself cannot be evaluated. It has been shown that a hybrid turbulence model, known as Detached

Eddy Simulation (DES), can provide more accurate wake results for a full turbine geometry than RANS, but at lower computational cost than LES. This is achieved by applying a RANS model in the near-wall areas around the turbine, but resolving large-scale turbulence in other regions, in the manner of LES[7].

This paper is designed in two parts: firstly, a discussion and assessment of different metrics which can be used to define and assess the size, shape, and impacts of wakes. This allows wakes to be objectively compared between different cases, and it is envisaged that this could be used to inform designers of turbine arrays when making decisions about array layout. The second part of this paper applies these metrics to a specific CFD case, modelled using a full turbine geometry using a DES turbulence model, which has been validated against wake measurements from a flume[7]. This model is run for a range of seven tip-speed ratios representing a wide range of operating conditions including high-torque, -power and -thrust.

II. Simulation methodology

A. Turbulence model

To date, the majority of numerical research on tidal turbines and their wakes has been conducted using RANS turbulence models. These models recognise that, for most engineering flows, users are more interested in the time-averaged values of flow variables such as velocity, than the instantaneous values. RANS models are based on the idea that the instantaneous value of a flow variable, e.g. velocity, can be represented by its mean and a fluctuating component. This process is known as Reynolds decomposition, and is represented mathematically in equation 1.

$$u(t) = U + u'(t) \tag{1}$$

The Reynolds-decomposed variables are then substituted into the incompressible 3-dimensional Navier-Stokes equations. This yields the time-averaged Navier-Stokes equations for U, which are formally identical to the Navier-Stokes equations for instantaneous flow variables, with an additional term, $\tau_{ij} = -\rho\overline{u_i' u_j'}$, known as the Reynolds stresses. The Reynolds stresses represent the exchange of momentum between the mean and the fluctuating flow components, and must be modelled in order to close the Navier-Stokes equations and obtain a solution for U. Various schemes have been developed for the modelling of the Reynolds stresses, each with differing levels of complexity, from the mixing length model, through two-equation models such as the k-ε and k-ω through to the Reynolds Stress Model, which requires seven equations to be solved for closure to be achieved[8].

The advantage of RANS equations is that they provide a good compromise between computational cost and accuracy. They are well characterised, and it is known which ones perform best for different types of flow. Variations such as the k-ω SST model exist, which attempt to combine the best characteristics of the k-ε and k-ω models. However, these models struggle with flows which demonstrate a large turbulence length scale or a high degree of turbulence anisotropy like that shown to be present in the wake of a tidal turbine[9]. This is thought to be due to the reliance of two-equation RANS models on the Boussinesq approximation, which assumes isotropy of turbulence. This assumption is usually valid for small-scale turbulence, but it becomes less appropriate for larger turbulent length scales[8], such as those found at potential tidal energy sites[10]. In addition to this, the focus on time-averaged values means that some data regarding fluctuating quantities is unavailable.

A different approach to accounting for turbulent fluctuations is provided by LES. This approach applies a spatial filter to the Navier-Stokes equations, with fluctuations larger than the filter width (typically the local cell size) being resolved, and fluctuations smaller than the filter width being treated with a sub-grid scale model, in a way analogous to a RANS model. LES allows for much more information to be gathered about fluctuating quantities than RANS models. This is because the fluctuations themselves (or at least, the large ones) are directly resolved, allowing the user to carry out their own statistical analysis on them, in a way similar to how measurements in a flume would be analysed. In addition to this, treating large and small eddies differently means that LES can accurately model flows with large turbulence anisotropy and length scales. However, LES is significantly more computationally expensive than two-equation RANS models for two main reasons; firstly, LES has higher mesh requirements in boundary regions, and secondly, in order for converged statistical values of fluctuating quantities to be obtained, the model must be run for significantly more time steps.

The DES method used in this work is a hybrid turbulence model which endeavours to combine the advantages of LES in the wake region with RANS in near-wall areas in order to more accurately model the wake, whilst reducing computational expense to less than would be required for a pure LES model. This is achieved by recognising that, once averaging has been carried out (time averaging in the case of RANS, or spatial averaging for LES), information about the averaging method is lost, and both RANS and LES models become turbulence viscosity models. The DES model compares the local turbulence length scale to the local cell size, and uses this to decide to what extent the turbulence viscosity of the model should be modified from that obtained from a k-ω SST model (if at all). This results in a RANS model being applied in near wall areas, and LES-like behaviour being recovered in the wake region. Due to space requirements, the mathematics of the model will not be described in detail here, as the necessary information has been previously detailed in [7] and [11].

B. Model domain and boundary conditions

A domain was created in order to replicate the geometry of the recirculating flume at the Institut français de recherche pour l'exploitation de la mer (IFREMER) in Boulogne-sur-Mer. This flume has a working section approximately 4 m wide, 2 m deep and approximately 18 m in length (henceforth designated the x-, y- and z-directions respectively). The turbine itself has a 3-bladed, 0.5 m diameter rotor based on a

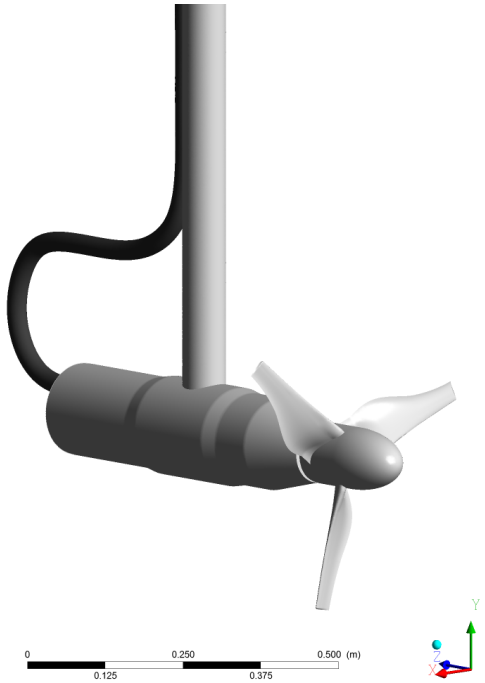

Fig. 1. The turbine modelled in this work.

Wortmann FX 63-137 section, with a twist of 30° from root to tip[12]. Speed control is provided by a motor contained within a stainless steel nacelle, 763 mm in length, with a maximum diameter of 160 mm. The turbine assembly is suspended at the mid-point of the cross-sectional area of the tank by a steel stanchion 71 mm in diameter. The turbine used is shown in Figure 1, and full details of its construction and control system can be found in [13].

The computational domain was created with the same width and depth as the tank, with a total domain length of 9 m. The turbine plane was located 1.5 m downstream of the inlet plane. The top face of the domain was given a free-slip condition, all other surfaces were subject to a no-slip condition. The inlet boundary was given a velocity normal to the inlet of 1.5 m/s, with a turbulence intensity of 1.75%, and length scale of 0.5 m (following the length scale definition in ANSYS Fluent®15.0). This matches the flow conditions measured during validation at the flume[7]. The velocity of 1.5 m/s was chosen as it has been shown to be large enough that turbine performance becomes independent of Reynolds number, allowing performance characteristics to be scaled using non-dimensional coefficients of power, thrust and torque[12]. A mesh independence study has been carried out for the turbine, wake region and flume walls to ensure that the mesh used is sufficiently fine that the results are dependent only on the numerical model used, and not on the grid.

The turbine rotor was enclosed in a cylindrical non-conformal subdomain region, coaxial to the axis of rotation. Rotation of the turbine was simulated by applying rotation to this subdomain via a sliding mesh scheme. This allows for fluctuating effects due to blade-stanchion interactions to be modelled, and is critical if the wake is to be accurately modelled.

Seven separate runs were made, differing only in the rotational velocity of the turbine. Rotational velocities were chosen in order to give tip-speed ratios of $\lambda = 1.5, 2.5, 3.0, 3.65, 4.0, 4.5$ and 5.5. $\lambda = 3.65$ was selected as it was previously found to be the point of maximum power coefficient (as defined by equation 3) for this turbine, and is therefore of particular interest. In addition to this, validation of the model has been previously carried out at a tip-speed ratio of $\lambda = 3.65$[7]. The range of tip-speed ratios was chosen in order to give comprehensive performance data for the turbine.

III. Wake measurement metrics

All objects which find themselves in a moving fluid will produce a wake. The wake of an object is a region of reduced fluid velocity, induced by the presence of the object and its effect of reducing the momentum of the fluid. Typically, the wake region will be more turbulent than the free-stream, as mixing takes place between the lower velocity wake region and the higher velocity free-stream. This mixing often starts as a thin, highly sheared layer between the wake region and the free-stream, which thickens and reduces in intensity as downstream distance increases. The whole wake tends to increase in width as energy and momentum is transferred from the free-stream to the wake. As distance downstream of the object increases, so the velocity of the wake region recovers until, in the far field, its average velocity become equal to the free-stream velocity.

Whilst this qualitative description of a wake will be widely recognised by flow-physicists, it is useful to develop quantitative metrics in order to quantify the length and the width of a wake. However, this is challenging due to the constantly changing nature of the wake (width increases whilst intensity decreases), and the highly turbulent nature of the wake region, which makes clearly defining wake length and width difficult.

A. Wake length

Wake length has been a subject of interest since the early days of wind turbine development. Fundamentally, it is important for the designer of an array of wind or tidal turbines to know how far downstream another turbine must be placed in order that there is enough kinetic energy available in the fluid flow for the downstream turbine to be economically viable. The most straightforward method of characterising the wake recovery is to examine the time-averaged axial velocity downstream of the turbine along its axis. This has the advantage of being easily measured in a series of single-point measurements in a wind tunnel, flume, or in the field. Such measurements can then be used to inform the placement of subsequent turbines, or compared to CFD simulations for validation purposes.

Whilst the simplicity of centreline velocity recovery holds appeal as a wake length metric, it only provides limited information about the kinetic energy available to a downstream

turbine. It is reasonable to assume that momentum transfer and therefore wake recovery will start from the outside of the wake, with the centreline being the last place to experience velocity recovery. Using the centreline velocity recovery would therefore over estimate the required downstream inter-turbine spacing, potentially reducing the number of turbines which could be placed in an area of fixed geographical extent, and therefore reducing the amount of energy yielded by such a site. It is also possible (as will be shown later) that the distribution of velocities in the wake might differ from one case to another, and this information is lost if only time-averaged centreline velocities are used. A more useful estimate of the energy available to a downstream turbine can be obtained by calculating the volumetrically averaged flow across the swept area of the turbine. This is obtained from CFD results by an area-weighted averaging of the mean axial velocity across the swept area of a turbine. Experimentally, this is more commonly obtained by measuring axial velocity in a rake of measurements perpendicular to the flow direction. A disc-integration procedure is then carried out to produce an area-weighted average for these results[14][7].

Regardless of whether centreline or volumetric averaged velocities are used, it is to be expected that the transfer of energy and momentum will be such that the velocity in the far wake will recover asymptotically to the free stream velocity. If this is the case, then the wake will only be fully recovered as the distance downstream of the turbine tends to infinity. To avoid this problem, it is customary to select an arbitrary threshold (for example, 90% wake recovery), after which, the wake is said to be 'recovered'.

B. Wake width

Defining and quantifying the cross-stream extent to which the wake disturbs the surrounding flow is more problematic than defining the wake length. Initially, the wake region of high velocity deficit is separated from the free-stream by a thin, highly sheared region. However, as the wake continues to develop downstream, this shear layer thickens as mixing and momentum transfer occurs between the free-stream and the wake. This thickening of the shear region occurs both inwards, toward the turbine centre axis, as well as outwards into the free-stream flow. At the same time, the flow velocity in the wake region is recovering, meaning that the wake is becoming more similar to the free-stream, and therefore the disturbance it is causing to the surrounding flow reduces. Further downstream in the far-wake region, the wake spreads to be significantly wider than the turbine, but the difference between flow this region and undisturbed free-stream flow is small. This combination of factors leads to difficulties when attempting to precisely quantify the width of a wake, therefore, in this work, three different possible metrics are examined and evaluated.

1) Width based on the point of maximum shear: The free-stream undisturbed flow, and the core wake region are separated by a region of velocity shear whose shape is approximately that of the surface of a cylinder. As discussed above, this region becomes thicker as a wake develops in the downstream direction and the strength of this shear decreases. One option is to define the width of the wake as the distance between the two points of maximum shear on either side of the wake. In this case, shear is defined as the rate of change of axial velocity in the cross stream direction.

2) Width based on a fixed threshold value: As mentioned in III-A, it is customary to set an arbitrary threshold for velocity recovery (e.g. 90%) in order to give a definition of a wake length. It is possible to use a similar method in order to define a wake width. In essence, a wake is a region of un-recovered axial velocity, when compared to the free-stream velocity. This method defines the wake width as being the width of the region which has not yet reached the threshold recovery level. Once the complete wake region has surpassed this recovery threshold, then the width of the wake becomes zero. For this work, the threshold used is 90% velocity recovery, although it should be noted that any arbitrary threshold may be used.

3) Width based on full-width half-minimum (FWHM): The cross-stream extent of a wake may be measured in a flume experiment by taking a rake of measurements of axial velocity in a cross-stream direction. This produces a 'bucket' shaped velocity profile for each rake. Borrowing techniques from signal processing for the evaluation of the width of a peak in a signal, a 'full-width half-minimum' method is employed. This method evaluates the width of a peak (or in this case, the inverted peak or 'bucket'), by taking into account the maximum magnitude of the deviation in signal - in this case, maximum velocity deficit at this point in the wake. The width of the wake is then defined as the width of the velocity profile which has recovered to half the deficit of the maximum measured for that velocity profile. In effect, the full-width of the profile, at half the maximum velocity deficit. This method may also be considered to be using a threshold value of recovered velocity in order to evaluate the wake width, but, in contrast to the fixed threshold method, the FWHM method takes into account the local maximum velocity deficit at this point in the wake.

C. Swirl

Swirling flows are those in which tangential (rotational) momentum is transferred in the axial direction. Such flows have been studied due to their importance in areas such as flame stability and mixing in combustors[15], and the strength of swirl in a jet has been shown to affect jet growth, entrainment and decay[16]. Swirl provides another metric which can be used to examine turbine wakes, as it can provide an insight into wake mixing and recovery processes, and it has been examined in previous CFD studies using a RANS turbulence model[17].

Lilley[16] defined swirl as follows:

$$S = \frac{G_\phi}{G_x r} \tag{2}$$

Where S is the non-dimensionalised swirl number, G_ϕ is the axial flux of angular momentum, and G_x is the axial flux of linear momentum. Lilley defined r as the distance from the

axis of rotation to the geometry edge; in this case, the turbine radius has been used.

IV. Results

Results are shown of wake length and width measurement metrics for a range of tip-speed ratios for the turbine discussed in section II. For each tip-speed ratio a model was run using a k-ω SST turbulence model for 1200 timesteps of 0.005 s, in order to initialise the flow-field for the DES run. The models were then run for a further 1200 timesteps of 0.005 s in order to allow the flow field to become statistically steady using the DES model. At this point, sampling for time-averaging was started, and the models run for a further 10 000 timesteps, representing 50 s of flow time, over which averaging was carried out in order to produce converged values for mean velocities in the wake region. Seven CFD runs at tip-speed ratios of $\lambda = 1.5, 2.5, 3.0, 3.65, 4.0, 4.5$ and 5.5 were carried out for the same inlet flow conditions, which are identical those used in the validation study[7]. For all wake results presented here, each metric will be accompanied by a figure showing the change of the value of that metric with flow-time. This provides an indication of how much flow time must be simulated in order to have confidence in the results. This is important for deciding how useful each metric is for time-limited CFD simulations. Results for wake length, width and swirl were calculated via scripts written in MATLAB 2016b, which operated on flow data obtained from the Fluent data file.

The torque and thrust data required for the calculation of the turbine performance characteristics (coefficients of power, torque and thrust) were gathered via a User Defined Function (UDF) which output this data to a text file for each timestep of the simulation. The results quoted below are based on analysis of the data obtained in the portion of the CFD run where time-averaging was taking place.

A. Turbine operating condition

Three commonly used metrics for describing turbine performance and operating condition are the non-dimensionalised power coefficient, C_P, thrust coefficient, C_T, and torque coefficient, C_θ, defined by equations 3, 4 and 5 respectively.

$$C_P = \frac{\tau\omega}{0.5\rho A v^3} \tag{3}$$

$$C_T = \frac{F_T}{0.5\rho A v^2} \tag{4}$$

$$C_\theta = \frac{\tau}{0.5\rho A v^2 r} \tag{5}$$

C_P, C_T and C_θ were calculated at every timestep, using torque and thrust data obtained via the UDF. Mean values were then calculated for the 50 s of flow time over which time averaging was carried out. The results are presented in Figures 2, 3 and 4 for C_P, C_T and C_θ respectively. The shape and position of these curves closely match that previously found for this turbine geometry[12]. Figure 2 shows, as in previous studies, that this turbine geometry has a peak C_P at a tip-speed ratio of 3.65, and a peak C_θ between a tip-speed ratio of 2.5 and 3.0. The curve of C_T contains no peak, but increases steadily to approximately $\lambda = 3.5$, and becomes essentially flat beyond $\lambda = 4$.

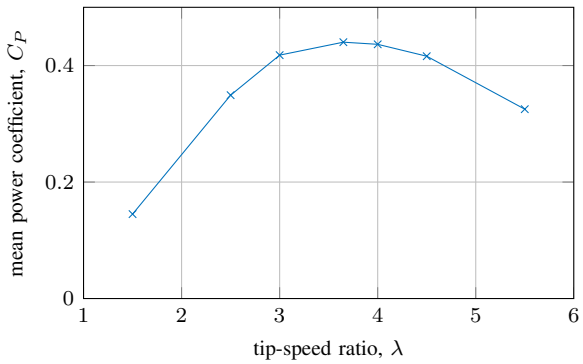

Fig. 2. Power curve for this turbine geometry. C_P is calculated as a mean over a time period of 50 s of flow time.

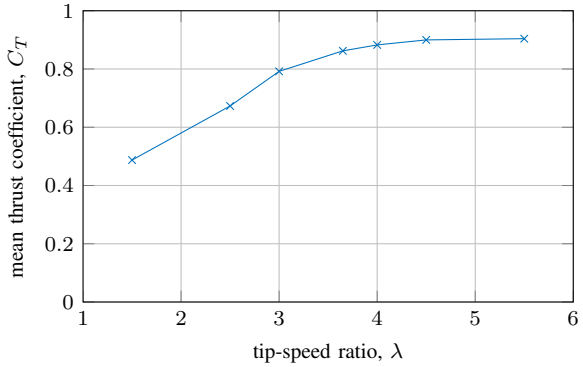

Fig. 3. Thrust curve for this turbine geometry. C_T is calculated as a mean over a time period of 50 s of flow time.

B. Wake length

Wake length was evaluated using time averaged values of axial velocity on planes perpendicular to the axis of the turbine, spaced at $1D$ intervals downstream of the turbine

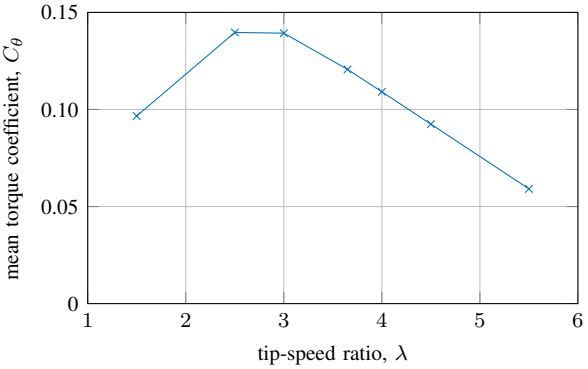

Fig. 4. Torque curve for this turbine geometry. C_θ is calculated as a mean over a time period of 50 s of flow time.

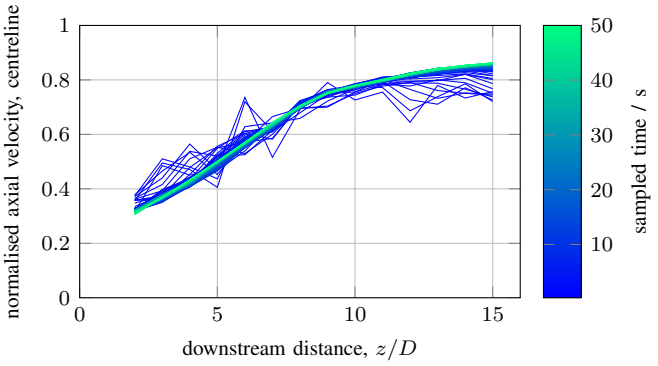

Fig. 5. Convergence of wake recovery curves (centreline velocity) curves for the $\lambda = 3.65$ case, showing how increasing sample time for time averaging affects the curve.

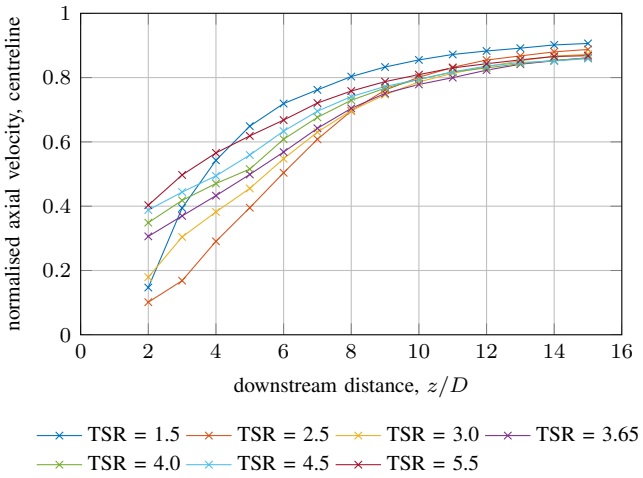

Fig. 6. Normalised axial velocity at centreline.

rotor, starting at a distance of $z/D = 2$. Centreline velocity recovery curves for the different tip-speed ratios are displayed in Figure 6, and axial velocities, volumetrically averaged across the swept area of the turbine are shown in Figure 8. The centreline wake recovery curves (Figure 6) show, with the exception of the $\lambda = 1.5$ case, that initial centreline recovery is higher as tip-speed ratio increases. However, after approximately $10D$ downstream, the centreline recovery becomes very similar. The $\lambda = 1.5$ case initially shows very low centreline recovery, but recovers very quickly, such that by $5D$ downstream, it has recovered to a greater extent than any of the other cases. The volumetric averaged velocity recovery curves exhibit slightly different trends. For the cases $2.5 \leq \lambda \geq 4.5$, the wake recovery curves are all very similar, with the lower tip-speed ratios demonstrating slightly higher initial recovery, up to approximately $4D$ downstream of the turbine plane, where they become similar to the other cases. The $\lambda = 1.5$ case shows much higher wake recovery for the entirety of the region shown, and the $\lambda = 5.5$ case starts off with a low initial recovery, then shows faster recovery than the $2.5 \leq \lambda \geq 4.5$ cases, before once more becoming similar to these after approximately $8D$. Convergence of the centreline velocities and volumetrically averaged velocities are represented in Figures 5 and 7 respectively, using the $\lambda = 3.65$ case as an example. Wake recovery curves are plotted at 0.25 s intervals for the 50 s over which time-averaging took place. These figures show that both curves converge very quickly to their final quoted values, indicating a high confidence in the stability of both of these metrics.

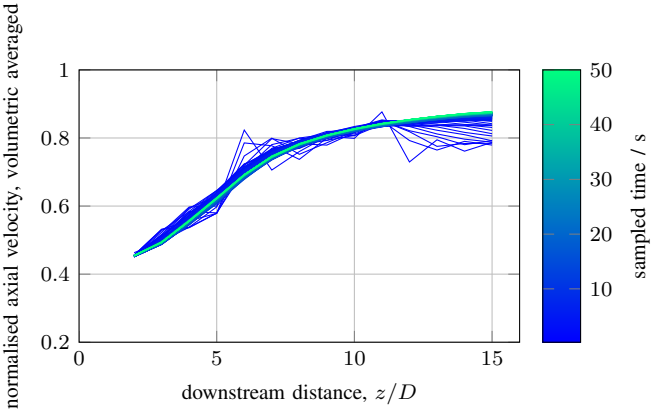

Fig. 7. Convergence of wake recovery curves (volumetric averaged velocity) curves for the $\lambda = 3.65$ case, showing how increasing sample time for time averaging affects the curve.

C. Wake width

Wake width was evaluated for each method discussed in III-B. This was carried out on a time-averaged axial velocity data on a horizontal plane containing the turbine axis. The data was extracted in a series of rakes spaced at $1D$ intervals downstream of the turbine rotor, starting at a distance of $z/D = 2$. Normalised wake widths using the fixed threshold method are shown in Figure 10, using the full-width half-minimum method in Figure 12 and using the point of maximum shear

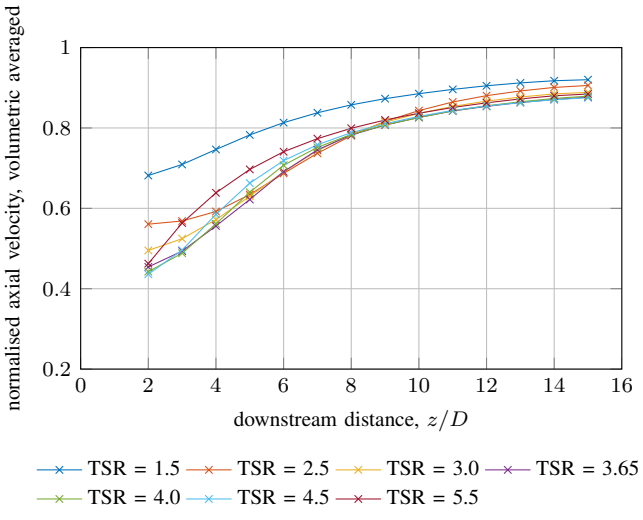

Fig. 8. Normalised axial velocity, volumetrically averaged across turbine swept area.

method in Figure 14. Wake width curves based on the fixed threshold method (Figure 10) all show a similar trend, with all except the curves for $\lambda = 4.5$ and $\lambda = 5.5$ showing a steady decrease in width as downstream distance from the turbine increases. This indicates that the width of the region which is less than 90% recovered is getting narrower as the wake recovers downstream of the turbine. The $\lambda = 4.5$ and $\lambda = 5.5$ cases show a slight increase in width until $z/D \approx 6$, before following the trend of the other curves. For all cases, a higher tip-speed ratio leads to a wider wake, with the differences being most pronounced in the low tip-speed ratio region. Wake width curves using the FWHM method (Figure 12) also indicate that a higher tip-speed ratio leads to greater wake width, but here the general trend is towards increasing wake width with downstream distance, indicating that the whilst the intensity of the wake might be decreasing as the wake recovers, the width of the region affected by the wake increases. Whilst there is an overall trend of increasing width with downstream distance, for the cases where $3.0 \leq \lambda \geq 4.5$ the width appears to first narrow, with a minimum width at $z/D \approx 6$ before the wake starts to widen. Convergence of the wake width curves for these two metrics can be seen in Figures 9 and 11, using the $\lambda = 3.65$ case as an example. These show that these metrics are well converged, with very little change visible beyond a sample time of 30 s, allowing a high confidence in the stability of both these metrics.

Wake width curves using the maximum shear definition of wake width (Figure 14) are much less clearly defined, and the curves appear to be much less well converged. This is supported by the evidence of Figure 13, which indicates poorly converged values in the region $z/D \geq 6$, with significant fluctuations in width even after longer sample times. For downstream distances $z/D \leq 5$, the metric yields good convergence, allowing a higher confidence to be had for this region. It appears that, following the trends in the other width measurement metrics, higher tip-speed ratios correspond to wider wakes when this method is used. However, the trend is much weaker than that shown by the other two methods. Similarly, there is a slight trend to an increase in wake width with increasing downstream distance for all cases. For tip-speed ratios greater than 2.5, widths are very similar in the region $2 \leq z/D \geq 5$. This also corresponds to the region of greatest convergence when compared with Figure 13. This indicates that the point of maximum shear is indeed located in the same place for all these cases.

D. Swirl

Wake swirl was calculated as defined by Lilley[16]. This was carried out on time-averaged data for velocity, on planes perpendicular to the axis of the turbine, spaced at $1D$ intervals downstream of the turbine rotor, starting at a distance of $z/D = 2$. This was carried out across the swept area of the turbine ($r = 0.25$ m). The results are shown in Figure 16. This shows the highest swirl is found in the wakes at tip-speed ratios of 2.5, 3.0 and 3.65, with tip-speed ratios of 5.5 and 1.5 demonstrating the least swirl. These correspond to the

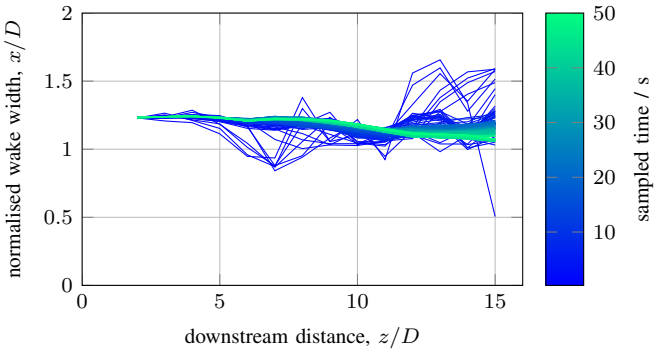

Fig. 9. Convergence of width measurement based on the fixed threshold method for the $\lambda = 3.65$ case, showing how increasing sample time for time averaging affects the curve.

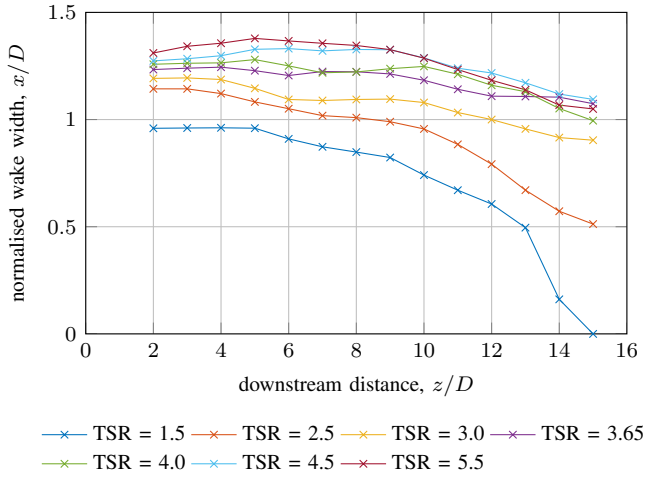

Fig. 10. Normalised wake width, using the fixed threshold method, based on a threshold of 90% wake recovery.

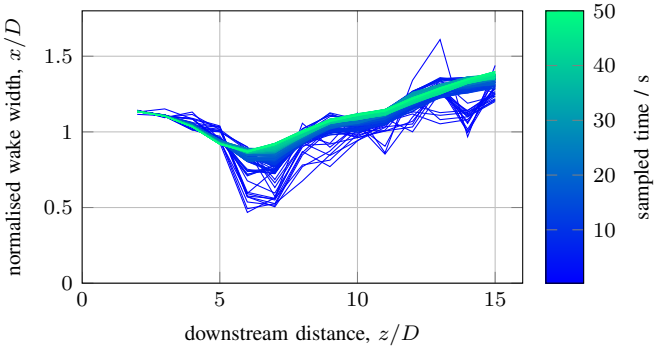

Fig. 11. Convergence of FWHM method for the $\lambda = 3.65$ case, showing how increasing sample time for time averaging affects the curve.

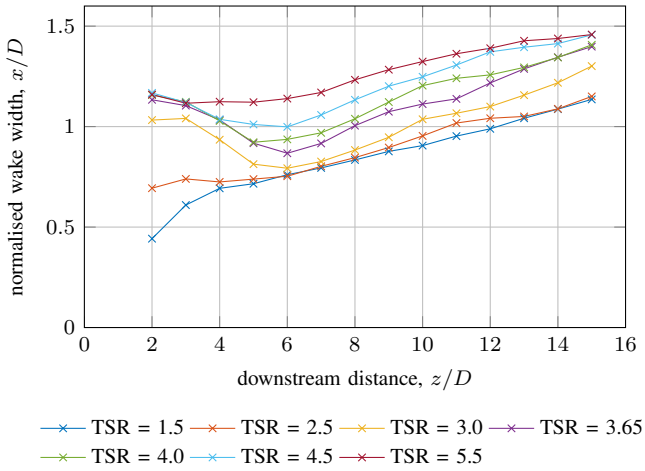

Fig. 12. Normalised wake width, using the full-width half-minimum method.

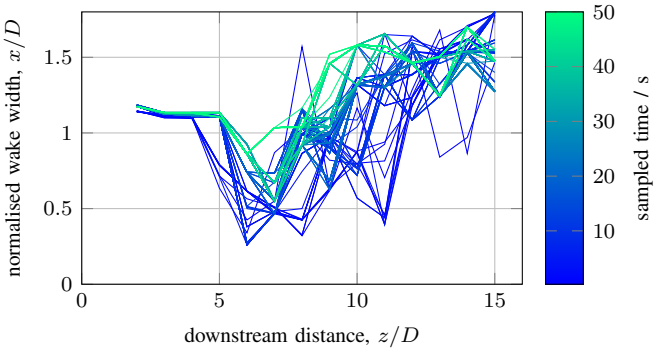

Fig. 13. Convergence of width measurement based on the maximum shear method for the $\lambda = 3.65$ case, showing how increasing sample time for time averaging affects the curve.

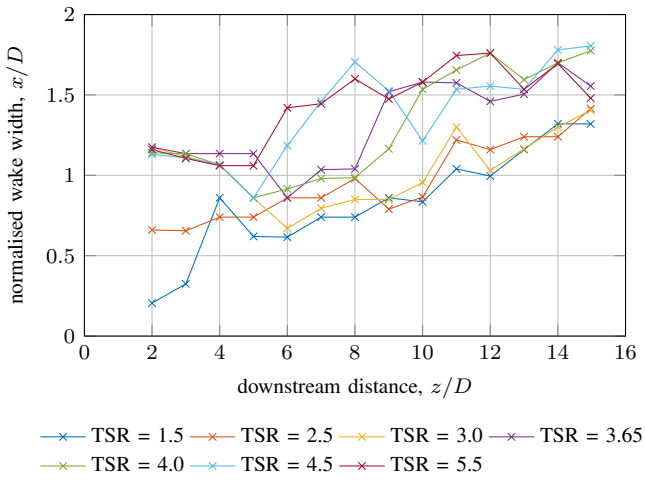

Fig. 14. Normalised wake width, using the point of maximum shear.

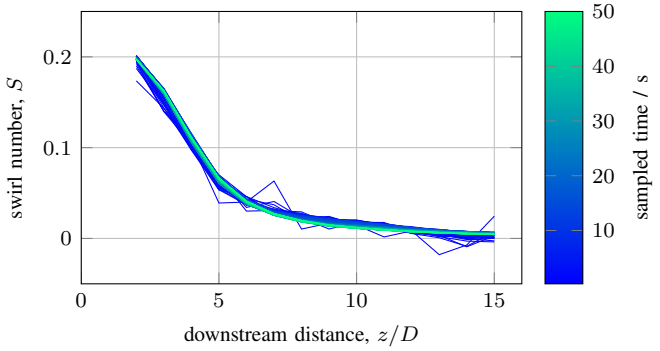

Fig. 15. Convergence of swirl number curves for the $\lambda = 3.65$ case, showing how increasing sample time for time averaging affects the curve.

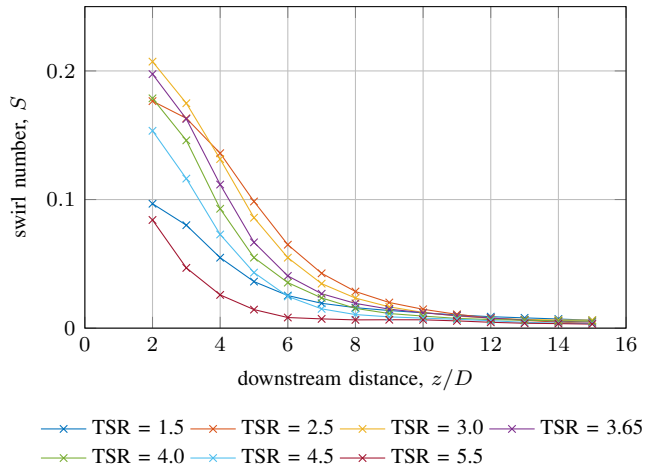

Fig. 16. Wake swirl number.

tip-speed ratios in the regions of highest and lowest C_θ values respectively. Figure 15 presents the convergence of the swirl curve for the $\lambda = 3.65$ case, and shows the swirl number values to be well converged in the wake region.

V. Discussion

A. Wake length and Tip-Speed Ratio

The two charts showing wake recovery (Figures 6 and 8), when taken together, provide a large amount of information about the wake. A comparison of the two gives an indication of the uniformity of the flow in the wake region. Where the two charts show similar values, then the wake is more uniform, but where there are differences, then this indicates that the centreline value is very different from the average. These differences arise due to the thrust developed by the turbine at different operating conditions. At low values of λ, the thrust produced by the blades of the turbine is low. This means that the wake deficit is in large part due to the drag from the nacelle, rather than that of the blades. This leads to the difference between Figures 6 and 8 for the $\lambda = 1.5$ case, particularly in the near wake region, where there has been little opportunity for mixing to take place. The centreline chart is

heavily influenced by the drag from the turbine nacelle, and thus recovery is very low. For the volumetrically averaged chart, the whole of the wake area is used for the calculation, and the large majority of this is not influenced by the nacelle, but rather, from the blades. The thrust on the blades at this tip-speed ratio is very low. Therefore, when volumetrically averaged, the wake recovery is high.

In addition to the $\lambda = 1.5$ case, the $\lambda = 5.5$ case differs significantly between Figures 6 and 8. The $\lambda = 5.5$ case shows the highest initial centreline velocity recovery, but is one of the lowest cases for initial volumetrically averaged velocity recovery. This is due to a reverse of the phenomenon which was observed in the $\lambda = 1.5$ case. The high tip-speed ratio case demonstrates the highest thrust, which comes primarily from thrust on the outer portions of the blades. This not only leads to the flow being diverted outside and around the turbine (increasing wake width), but also leads to flow being diverted to the *inside*, towards the nacelle. This promotes a rapid recovery of the wake along the turbine centreline, but with an overall lower rate of wake recovery when a volumetrically averaged approach is used.

It should also be noted that the extreme cases of $\lambda = 1.5$ and $\lambda = 5.5$ show the greatest volumetric averaged wake recovery from approximately $z/D = 4$ onwards, whilst the $\lambda = 3.65, 4$ and 4.5 cases generally show the lowest rates of recovery. More energy has been extracted from the flow for these cases, which leads to lower velocities in the wake region. Nonetheless, other than the extreme cases of $\lambda = 1.5$ volumetrically averaged velocities become very similar for all cases from $z/D \approx 7$. This suggests that, for array designers, turbine operating condition probably has little practical effect on wake length as it is unlikely that turbines will be placed less than $8D$ downstream of each other due to the lack of overall wake recovery.

B. Wake width and Tip-Speed Ratio

Wake width appears to increase, regardless of the metric used, as the tip-speed ratio increases. This follows the trend of C_T, and suggests that a turbine presenting more resistance to the flow will tend to cause more flow to divert around it. The widths in the far wake region for the four highest thrust cases ($\lambda = 3.65, 4.0, 4.5$ and 5.5) are very similar (for the FWHM and fixed threshold method), which is reproduced in the flattening of the C_T curve in this region. The same general trends can be seen in the far wake of the max shear width method (Figure 14), but the results in this region are very sensitive to fine changes in shear, and therefore the authors do not recommend using this technique. This sensitivity is due to the shape of the velocity profiles, which are similar for all tip-speed ratios beyond approximately $z/D = 7$. These profiles are approximately v-shaped, leading to a large cross-stream extent with almost an identical shear. This leads to the convergence difficulties seen in Figure 13. A slight deviation anywhere along this curve can lead to large changes in the position of the point of maximum shear, without any fundamental change to the curve itself. For $\lambda \geq 3.0$, and downstream distances of $z/D \leq 4$, the results are well converged. This is because, for these tip-speed ratios in this region, the velocity profiles are shaped like an inverted top-hat. This means that the point of maximum shear occurs within a very small cross-stream region. This clearly defined point of maximum shear means that the width metric is less susceptible to small deviations in this region.

In section III-B it was discussed that both the threshold width, and FWHM methods can both be thought of as methods which use a velocity threshold to define the wake width. In the case of the fixed threshold method, this velocity threshold is arbitrarily set at 90% of the free stream velocity, whereas the FWHM bases the velocity threshold it uses on the maximum velocity deficit at that point in the wake. The difference that this makes can be clearly seen by comparing Figures 10 and 12. For all tip-speed ratios, with a fixed threshold velocity, the wake starts wide and gets narrower as downstream distance increases. This is due to the fact that wake recovery is caused by the mixing of the reduced velocity wake and the surrounding free-stream, and therefore occurs from the outside to the centre. For the $\lambda = 1.5$ case, the wake width at $z/D = 15$ reduces to zero by this definition, as the entire wake has recovered by more than 90%. In contrast to this, at $\lambda \geq 3.0$ for the FWHM method, the wake starts wide, then narrows at approximately $z/D = 6$ before widening again. This is due to a change in shape of the velocity profile from an inverted top-hat shape to a v-shape.

Combining the FWHM and fixed-threshold methods provides more information about the change in width of the wake as downstream distance from the turbine increase than either of these methods on its own. The FWHM method indicates that the wake width is increasing, but when this information is combined with that provided by the fixed threshold method, then it can be seen that the width of the region with a high velocity deficit is decreasing. This definitively shows that the wake width is increasing, but the strength of the wake is decreasing, and this kind of detailed information is crucial for array designers considering where to site their turbines.

C. Wake swirl and Tip-Speed Ratio

Figure 16 shows a decay in swirl number, of a shape characteristic of that in a vortex[16]. This indicates that the flux of rotational momentum decreases with respect to the flux of linear momentum as the wake develops downstream. Whilst the curves all demonstrate similar behaviour, some have a higher swirl number than others. The two cases with the highest amount of swirl are the $\lambda = 2.5$ and $\lambda = 3.0$ cases. These correspond to the two cases with the highest torque coefficients, as shown in Figure 4. The case with the lowest swirl is the $\lambda = 5.5$ case, which corresponds to the lowest torque coefficient case shown in Figure 4. This is to be expected, as if there is a higher torque on the turbine, then it follows that there this must be countered by a higher reaction torque on the flow, which expresses itself as an increase in rotational momentum. Accurate representation of rotation in the flow downstream of a turbine is important in array design,

as it could potentially alter the anticipated angle of attack of blades on downstream turbines, or could potentially be utilised by downstream turbines rotating in the opposite sense to their upstream counterparts.

VI. Conclusions and prospects

This study compares three different metrics which can be used to analyse the width of a turbine wake. Both the fixed threshold and FWHM methods have been demonstrated as capable of providing useful, albeit subtly different information about the wake width. The FWHM method indicates that the wake width increases with downstream distance. This shows that the area which is affected by the presence of the turbine increases with downstream distance, but it does not indicate the intensity of the wake at each point. In contrast to this, the fixed threshold method indicates that the wake width decreases with downstream distance. In fact, this method indicates that the area of the wake *which still has a particular intensity* decreases. Using these two methods allows the conclusion that, as downstream distance increases, the wake simultaneously broadens, and its intensity weakens – information of great interest to array designers. The third method of analysing the wake width; basing the width on the position of the point of maximum shear, was shown to be less reliable. This is due to the shape of the velocity profiles downstream of the turbine. In all cases, with $z/D \geq 6$, the velocity profiles develop into a v-shape, which means there is a large region over which the shear is almost constant. Consequently, very small changes in velocity can lead to a large shift in the calculated position of the wake edges, without changing the shape of the velocity profiles in a meaningful way. This leads to this method being extremely sensitive to small changes in velocity, and whilst the general trends of wake width obtained from this method are the same as with the other two methods (higher thrust corresponding to wider wakes), the convergence difficulties associated with this method mean that the authors do not recommend its use.

This work also shows that there is a strong correlation between turbine operating condition and wake length, width and swirl. The clearest trend is that turbine operation at a higher C_T can be expected to produce a wider wake overall. This is explained as a higher thrust on the turbine indicates a greater resistance to the flow, therefore more flow will be diverted around the turbine, making the wake wider. At lower values of C_T, There is less flow diversion, and therefore the wake remains narrower. The combination of the fixed-threshold method and the FWHM method provides a more detailed pictured still, and shows that whilst the overall area influenced by the wake increases with downstream distance, the strength of this effect decreases.

With regards to wake length, a pattern also emerges, relating the rate of wake recovery to turbine operating condition. For both centreline and volumetric averaged measurements, the cases at $\lambda = 1.5$ and 5.5 show the fastest overall wake recovery. The slowest initial rate of recovery of volumetric averaged velocity is demonstrated by the tip-speed ratios corresponding to maximum power extraction. However, with the exception of the extreme case of $\lambda = 1.5$, volumetric averaged velocities in all cases become extremely similar after approximately $8D$ downstream, and centreline velocities become extremely similar after approximately $10D$ downstream. This indicates that wake length is essentially independent of tip-speed ratio beyond these distances.

Acknowledgements

This work was performed using the computational facilities of the Advanced Research Computing @ Cardiff (ARCCA) Division, Cardiff University. The authors acknowledge the financial support provided by the Welsh Government and Higher Education Funding Council for Wales through the Sêr Cymru National Research Network for Low Carbon, Energy and the Environment.

References

[1] Jack Hardisty. Power intermittency, redundancy and tidal phasing around the United Kingdom. *The Geographical Journal*, 174:76–84, 2008.

[2] D.M. O'Doherty, A. Mason-Jones, C. Morris, T. O'Doherty, C. Byrne, P.W. Prickett, and R.I. Grosvenor. Interaction of marine turbines in close proximity. In *Proc. of 9th European Wave and Tidal Energy Conference (EWTEC), Southampton, UK*, 2011.

[3] AbuBakr S. Bahaj. Generating electricity from the oceans. *Renewable and Sustainable Energy Reviews*, 15(7):3399 – 3416, 2011.

[4] Steffen Wußow, Lars Sitzki, and Thomas Hahm. 3D-simulation of the turbulent wake behind a wind turbine. *Journal of Physics: Conference Series*, 75(1):012033, 2007.

[5] M.J. Churchfield, Y. Li, and P.J. Moriarty. A large-eddy simulation study of wake propagation and power production in an array of tidal-current turbines. *Phil. Trans. R Soc. A*, 371:20120421, 2013.

[6] T. Blackmore, W.M.J. Batten, and A.S. Bahaj. Influence of turbulence on the wake of a marine current turbine simulator. *Proc. R. Soc. A*, 470:20140331, 2014.

[7] T. Ebdon, D. O'Doherty, T. O'Doherty, and A. Mason-Jones. Modelling the effect of turbulence length scale on tidal turbine wakes using advanced turbulence models. In *Proc. of 12th European Wave & Tidal Energy Conference (EWTEC 2017)*, 27th Aug – 1st Sept. 2017.

[8] H.K. Versteeg and W. Malalasekera. *An Introduction to Computational Fluid Dynamics, The Finite Volume Method*. Pearson Education Limited, 2007.

[9] S.C. Tedds, I. Owen, and R.J. Poole. Near-wake characteristics of a model horizontal axis tidal stream turbine. *Renewable Energy*, 63:222–235, 2014.

[10] I.A. Milne, R.N. Sharma, R.G.J. Flay, and S. Bickerton. Characteristics of the turbulence in the flow at a tidal stream power site. *Phil Trans R Soc A*, 371:20120196, 2013.

[11] T. Ebdon, D. O'Doherty, T. O'Doherty, and A. Mason-Jones. Simulating Marine Current Turbine Wakes Using Advanced Turbulence Models. In *Proc. of 3rd Asian Wave & Tidal Energy Conference (AWTEC 2016)*, 24th–28th Oct. 2016.

[12] A. Mason-Jones. *Performance assessment of a Horizontal Axis Tidal Turbine in a high velocity shear environment*. PhD thesis, School of Engineering, Cardiff University, 2010.

[13] Matthew Allmark. *Condition Monitoring and Fault Diagnosis of Tidal Stream Turbines Subjected to Rotor Imbalance Faults*. PhD thesis, School of Engineering, Cardiff University, 2016.

[14] Paul Mycek, Benoît Gaurier, Grégory Germain, Grégory Pinon, and Elie Rivoalen. Experimental study of the turbulence intensity effects on marine current turbines behaviour. Part I: One single turbine. *Renewable Energy*, 66:729–746, 2014.

[15] O. Lucca-Negro and T. O'Doherty. Vortex breakdown: a review. *Progress in Energy and Combustion Science*, 27:431–481, 2001.

[16] David G. Lilley. Prediction of inert turbulent swirl flows. *AIAA Journal*, 11(7):955–960, 1973.

[17] C.E. Morris, D.M. O'Doherty, A. Mason-Jones, and T. O'Doherty. Evaluation of the swirl characteristics of a tidal stream turbine wake. *International Journal of Marine Energy*, 14:198–214, 2016.